Journal of Materials Chemistry C

Accepted Manuscript

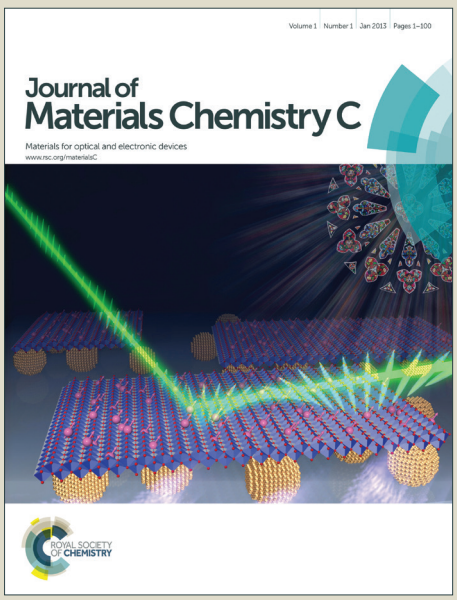

ROYAL SOCIETY OF CHEMISTRY

www.rsc.org/materialsC

A bridged low band gap A-D-A quaterthiophene as efficient donor for organic solar cells

François Baert,[a] Clément Cabanetos,[a] Antoine Leliège,[a] Eva Kirchner,[a] Olivier Segut,[a] Olivier Alévêque,[a] Magali Allain,[a] Gijun Seo,[b] Sungyeop Jung,[b] Denis Tondelier,[b] Bernard Geffroy,[c] Jean Roncali,[a] Philippe Leriche[a] and Philippe Blanchard*[a]

[a] MOLTECH-Anjou, CNRS UMR 6200, University of Angers, Group Linear Conjugated Systems, 2 Bd Lavoisier, 49045 Angers, France. E-mail: philippe.blanchard@univ-angers.fr

[b] LPICM, Ecole Polytechnique, CNRS UMR-7647, 91128 Palaiseau, France

[c] LICSEN, CEA Saclay IRAMIS/NIMBE, 91191 Gif sur Yvette, France

Abstract: α,ω-Bis(dicyanovinyl)quaterthiophene **1** with a median 4,4-diethyl-4*H*-cyclopenta[2,1-*b*:3,4-*b*']dithiophene has been synthesized. UV-Vis absorption data show that the covalent bridging of the inner 2,2'-bithiophene leads to a significant reduction of the HOMO-LUMO gap essentially due to an increase of the HOMO level as confirmed by electrochemical and theoretical results. X-ray diffraction analysis of a single crystal of **1** shows that except for the out-of-plane ethyl groups, the conjugated system displays a quasi-planar geometry while the molecular packing exhibits strong π-stacking interactions and multiple short intermolecular contacts.

Quaterthiophene **1** has been used as active donor material in organic solar cells of various architectures including bi-layer planar hetero-junctions and hybrid co-evaporated bulk hetero-junctions with C_{60} as electron acceptor material. A maximum conversion efficiency of 4.30% is obtained with a hybrid co-evaporated device. These results are discussed in terms of structure-properties relationships with reference to the open-chain parent α,ω-bis(dicyanovinyl)quaterthiophene **2**.

Introduction

Small π-conjugated molecules containing electron-donating and electron-accepting units are a focus of considerable current interest as active donor materials in organic photovoltaics (OPV).[1] Although solution-processed OPV cells based on low band gap conjugated polymers have reached power conversion efficiencies (*PCE*) in the range of 9.0% for single junction devices,[2] discrete molecules present some advantages in terms of reproducibility of synthesis and purification and analysis of structure-properties relationships.[1,3] While initial prototypes of solution–processed molecular bulk hetero-junction (BHJ) exhibited modest performance,[4] the field has rapidly progressed and recently, several groups have reported *PCE* in the 7.0-8.0% range by combining molecular donors of sophisticated design with $PC_{71}BM$ as acceptor and specific additives.[5,6,7] In parallel, OPV cells based on vacuum-deposited molecular donors have also recorded considerable progress and *PCE* of 6.0-7.0% have been reported for multi-layer planar hetero-junction (PHJ) cells combining molecular donors and C_{60} or C_{70} as acceptor.[8-10] An interesting advantage of vacuum-deposited PHJ cells is that the absence of solubility requirements allows the design of simpler donor structures of lower molecular weight that are generally more stable than their soluble versions.

Oligothiophenes (nTs) have been widely used as *p*-type organic semiconductors in organic (opto)electronics devices such as OFETs, OLEDs and OSCs.[11-14] While the maximum *PCE* of cells based on pure nTs has remained at a modest level for a long time,[15-17] a *PCE* of 1.50% was recently reported for a hybrid co-evaporated cell with 6T as donor, C_{60} as acceptor and an exciton-blocking buffer layer.[18]

Bäuerle, Leo and co-workers have intensively investigated various series of nTs end-capped with electron-accepting dicyanovinyl (DCV) groups as donor materials in multi-layer PHJ cells prepared by vacuum-process.[19] In particular they analyzed the effects of alkyl substituents on various series of DCV-end-capped nTs and highlighted the key role of the

number and position of short alkyl groups on the crystallographic structure and OPV performance of the donor material. Thus, a highest *PCE* of 6.90% has been reported for an optimized multi-layered cell with a 5T with a median 3,4-dimethylthiophene unit.[9]

Quaterthiophene (4T) has been identified as an interesting *p*-type organic semiconductor already in 1990.[20] In fact, together with other short-chain oligothiophenes,[21] 4T could represent an interesting starting point for the design of OPV materials combining low molecular weight and structural simplicity.[1h,22]

We have extensively investigated the rigidification of π-conjugated thiophene-based systems by covalent bridging and demonstrated that this approach represents a powerful tool for the control of their electronic properties.[23] Recently the extension of this approach to the electron-withdrawing end-group of small push-pull molecular donors has shown to significantly improve their performance in OPV cells.[24]

In this work, we report on the synthesis and characterization of a DCV-end-capped 4T in which the inner 2,2'-bithiophene block is rigidified by covalent bridging (**1**) (Chart 1). Note that quaterthiophene derivatives with similar structures have been previously reported as active materials for n-type organic field-effect transistors[25] and OPV.[26] The optical, electrochemical and thermal properties of titled compound **1** have been investigated and the crystallographic structure of a single crystal has been analyzed. The potential of compound **1** as donor material has been evaluated stepwise, as already reported,[27] first on vacuum-processed bi-layer PHJ and then on co-evaporated BHJ using C_{60} as acceptor. The results are discussed in terms of structure-properties relationships using the open-chain compound **2** as reference.

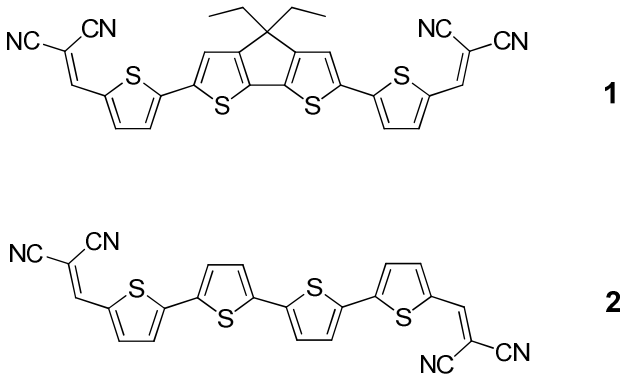

Chart 1 Molecular structures of the target compound **1** and the open-chain reference compound **2**.

Results and discussion

The reference compound **2**[19b] and 4,4-diethyl-4*H*-cyclopenta[2,1-*b*:3,4-*b*']dithiophene **3**[28] were prepared according to the literature. The two short ethyl chains of **3** were introduced to increase the solubility of the target compound **1** while still allowing intermolecular interactions. The synthesis of **1** is described in Scheme 1. Lithiation of **3** with *n*-butyllithium and subsequent quenching with trimethylstannyl chloride gave the bis(stannyl) reagent **4**. A twofold Stille cross-coupling[29] with 2-((5-bromothiophen-2-yl)methylene)malononitrile **5**[19c] led to the target compound **1**. However, as shown by mass spectrometry, this compound contains traces of a sexithiophene homologue by-product difficult to separate and resulting from an undesired homocoupling reaction of **4** followed by a double Stille reaction with **5**. In order to circumvent this problem, we used an alternative route based on the Stille coupling of 5-bromothiophene-2-carbaldehyde **6** with **4**. In that case, the sexithiophene by-product is separated by column chromatography and the bis-aldehyde product **7** is obtained in 87% yield. Finally, a Knoevenagel condensation of **7** with malonodinitrile yielded the target compound **1** (93%). The presence of the two ethyl chains on compound **1** significantly increases its solubility compared to **2** thus allowing its purification by column chromatography.

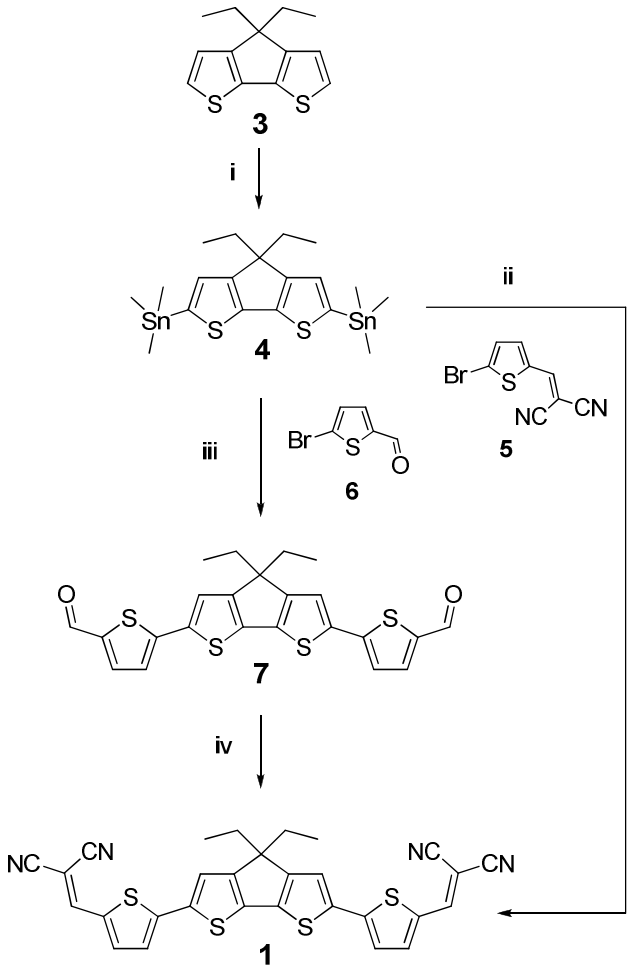

Scheme 1 Synthesis of compound **1**. Reagents and conditions: (i) *n*-BuLi (2.5 eq.), Me_3SnCl (2.5 eq.), THF, -78°C (96%); (ii) $Pd(PPh_3)_4$ (0.05 eq.), DMF, 80°C; (iii) $Pd(PPh_3)_4$ (0.05 eq.), DMF, 80°C (87%); (iv) $CH_2(CN)_2$ (3 eq.), Et_3N (0.1 eq.), $CHCl_3$ (94%).

Single crystals suitable for X-ray diffraction were grown by the slow evaporation of a $CHCl_3$ solution of compound **1**. The later crystallizes in the triclinic space group *P*-1 with one independent molecule of **1** and one independent molecule of $CHCl_3$ per asymmetric unit (see ESI, Table S1, Fig. S7-S9). Fig. 1 shows that the two terminal thiophene rings of **1** adopt two different conformations, *syn* or *anti*, relatively to the central bridged unit with the DCV units pointing toward opposite directions with respect to the main axis of the 4T backbone. As generally observed, the DCV groups adopt a *cis* conformation relatively to the sulphur atom of their vicinal thiophene units.[19b,24b]

Except for the two ethyl chains of the methylene bridge perpendicularly to the main molecular plane, molecule **1** is almost planar with a 0.03 Å RMS deviation from planarity. As expected, the bridged bithiophene core is fully planar. A slight deviation from planarity results from a small dihedral angle C12-C13-C14-C15 of 5.6° between the bridged core and the terminal thiophene unit in *syn* conformation whereas a dihedral angle C3-C4-C5-C6 of 1.1° is observed for the thiophene ring in *anti* conformation.

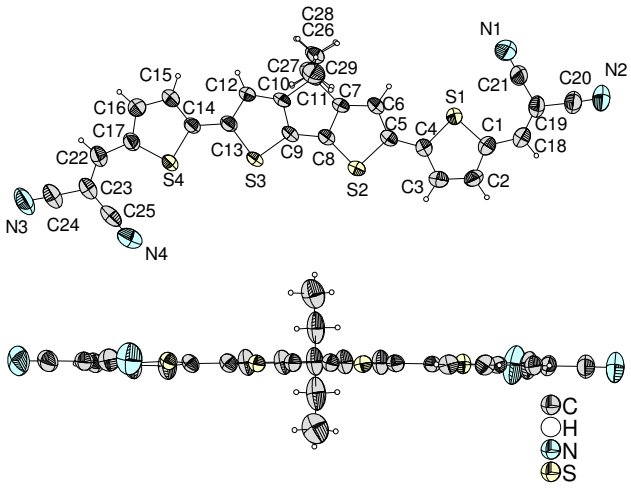

Fig. 1 ORTEP views of compound **1** with ellipsoids drawn at 50% probability level.

Fig. 2 shows that molecules **1** are regularly stacked along the *a* axis with a parallel orientation and a head-to-tail arrangement with respect to the diethyl chains. The short mean intermolecular distances inside the column d_1 = 3.577 Å and d_2 = 3.541 Å are consistent with a compact packing associated with π-π stacking interactions. Detailed analysis of the structure reveals multiple S···S distances shorter than twice the van der Waals radius of sulphur (3.70 Å). For instance the sulphur atoms of the bridged blocks in a stack are distant of 3.600(1) Å ($d_{S2\text{-}S3'}$) and 3.646(1) Å ($d_{S3\text{-}S3'}$). On the other hand, an intermolecular S···S distance $d_{S2\text{-}S4'}$ of 3.650(1) Å is observed between a sulphur atom of a bridged bithiophene and a terminal thiophene. Molecules **1** form an almost layered structure approximately in the *bc* plane.

Indeed, molecules **1** are nearly coplanar with small offsets of coplanarity of d_3 = 0.531 Å and d_4 = 0.496 Å between neighbouring molecules of different columns.

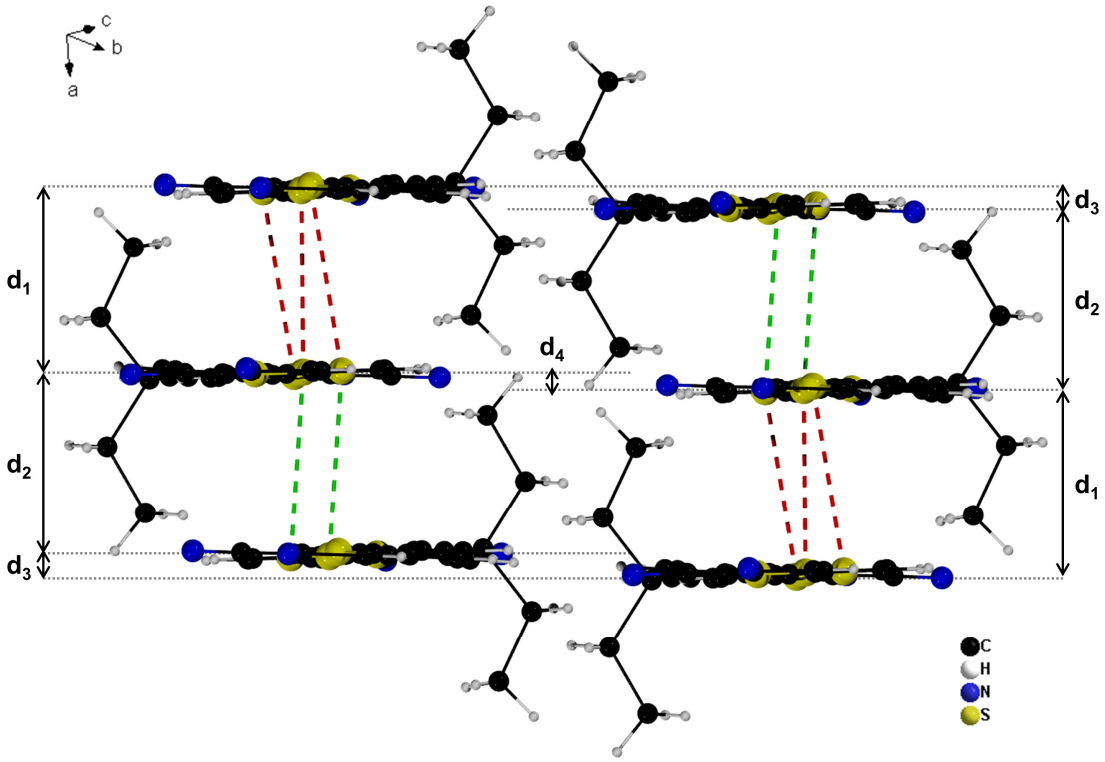

Fig. 2 Molecular packing of molecules **1** along the *a* axis showing the mean intermolecular distances (d_1 = 3.577 Å and d_2 = 3.541 Å) and S···S contacts (green and red dashed lines) shorter than the sum of van der Waals radii of sulphur atom (3.70 Å) inside a column. The offsets of coplanarity between neighbouring molecules (d_3 = 0.531 Å and d_4 = 0.496 Å) are also indicated. ($CHCl_3$ molecules have been omitted for clarity).

The view in the *bc* plane shows the overlap of two neighbouring molecules in the stack (Fig. 3). Again, a head-to-tail organization is clearly apparent. Two consecutive molecules of a column are slightly shifted along and perpendicular to the main molecular axis so that the two related bridged units do not overlap perfectly although short S···S intermolecular contacts exist as already mentioned. Overlaps between terminal thiophene rings and DCV units are observed with some short intermolecular C···C distances ($d_{C4\text{-}C23'}$ = 3.759(6) Å, $d_{C4\text{-}C22'}$ = 3.590(6) Å and $d_{C3\text{-}C22'}$ = 3.590(7) Å) in agreement with the existence of π-π stacking. It is worth noting that the perpendicular orientation of the two ethyl chains

relatively to the plane of the conjugated system does not prevent close molecular packing thus allowing intermolecular electronic coupling in the stacks.

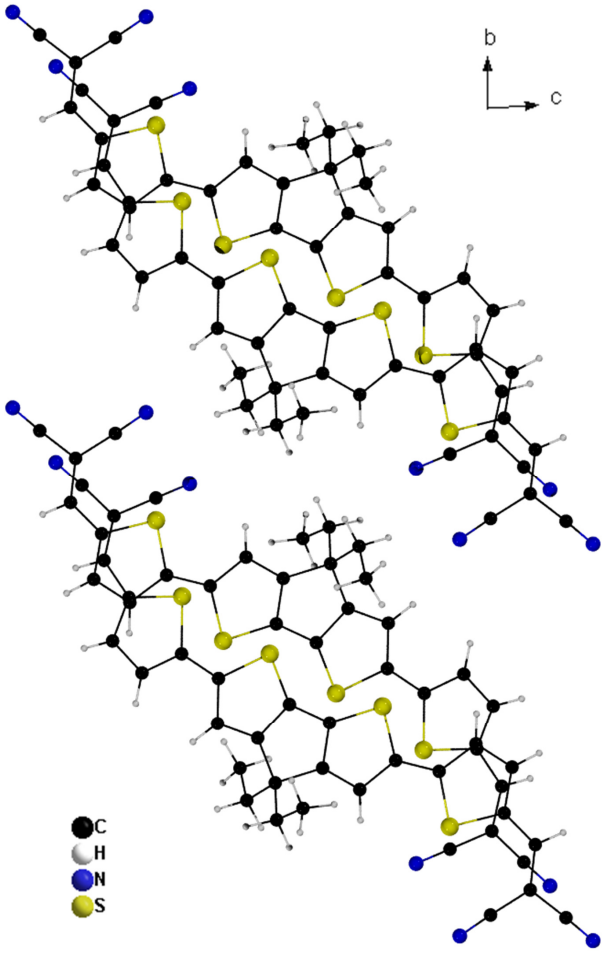

Fig. 3 Overlap of molecules **1** viewed in the *bc* plane.

C-H···N hydrogen bonding interactions are represented in Fig. 4. In fact, short intermolecular N···H contacts are observed between nitrogen atoms of the DCV nitrile group and vinylic hydrogen atoms of DCV ($d_{N3\text{-}H18}$ = 2.732(7) Å and $d_{N2\text{-}H22}$ 2.398(6) Å) or thiophenic hydrogen atoms of the bridged bithiophene ($d_{N1\text{-}H12}$ = 2.480(6) Å). Such hydrogen bonding interactions consolidate the crystal packing in a 2D network as observed for **2**.[19b]

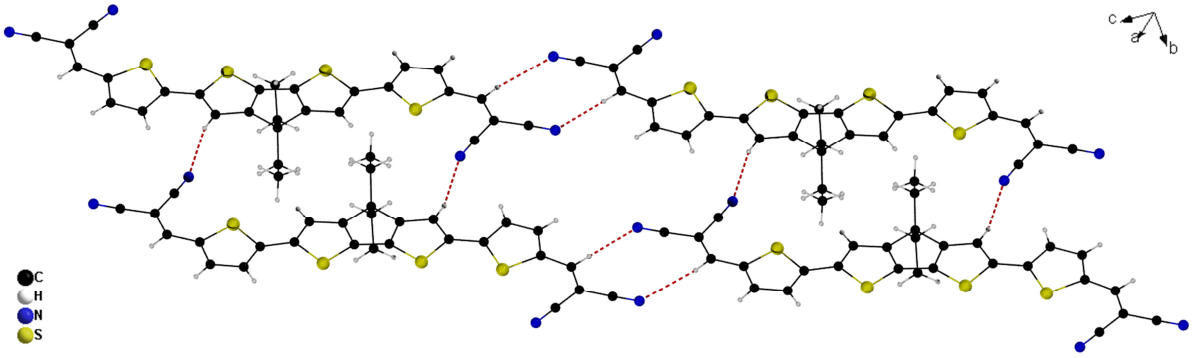

Fig. 4 Short N···H intermolecular contacts (red dashed lines) between molecules of **1**.

The thermal properties of **1** have been analyzed by differential scanning calorimetry (DSC) and thermogravimetric analysis (TGA). The first DSC trace shows a sharp endothermic peak with an onset at 303°C corresponding to the melting point of **1** (Fig. S10). At higher temperatures, the DSC trace exhibits an intense exothermic peak with an onset at 384°C assigned to the beginning of decomposition. The high thermal stability of **1** was confirmed by TGA which indicates a decomposition temperature T_d, defined at 5% weight loss, of 368°C in close agreement with DSC data.

Thermal evaporation of **1** under vacuum readily affords homogenous thin-films without any sign of decomposition as confirmed by MALDI-TOF and UV-Vis analysis of a re-dissolved film. Vacuum-deposited thin-films of **1** or **2** on glass at room temperature with 15 nm or 80 nm thickness have been analyzed by X-ray diffraction (XRD). In our conditions (see ESI), the absence of diffraction peaks, in each case, suggests the very low degree of crystallinity of the films.

The electronic and electrochemical properties of **1** have been analyzed by UV-vis spectroscopy and cyclic voltammetry. The absorption spectrum of compound **1** in CH_2Cl_2 exhibits a broad band extending from 450 to 700 nm attributed to a π-π* transition with an absorption maximum λ_{max} at 581 nm (Fig. 5, top). Comparison with compound **2** shows that the bridging of the central 2,2'-bithiophene block leads to a 65 nm bathochromic shift of λ_{max},

in agreement with a reduction of the HOMO-LUMO gap, while the molar extinction coefficient ε increases from 66400 to 80300 $L.mol^{-1}.cm^{-1}$. The absorption spectrum of a thin film of **1** evaporated on glass presents a 28 nm red shift of λ_{max} and a broadening of the absorption band compared to the solution spectrum (Fig. 5, bottom). The well-defined shoulder observed at *ca*. 660 nm is attributed to intermolecular π-interactions in the solid state. Optical band gaps of 1.68 and 1.82 eV have been estimated respectively from the long wavelength absorption edge of thin-films of **1** and **2**. Consistently with the results obtained in solution, the absorption coefficient of the films increases from 1.59×10^5 cm^{-1} for **2** to 1.83×10^5 cm^{-1} for **1**.

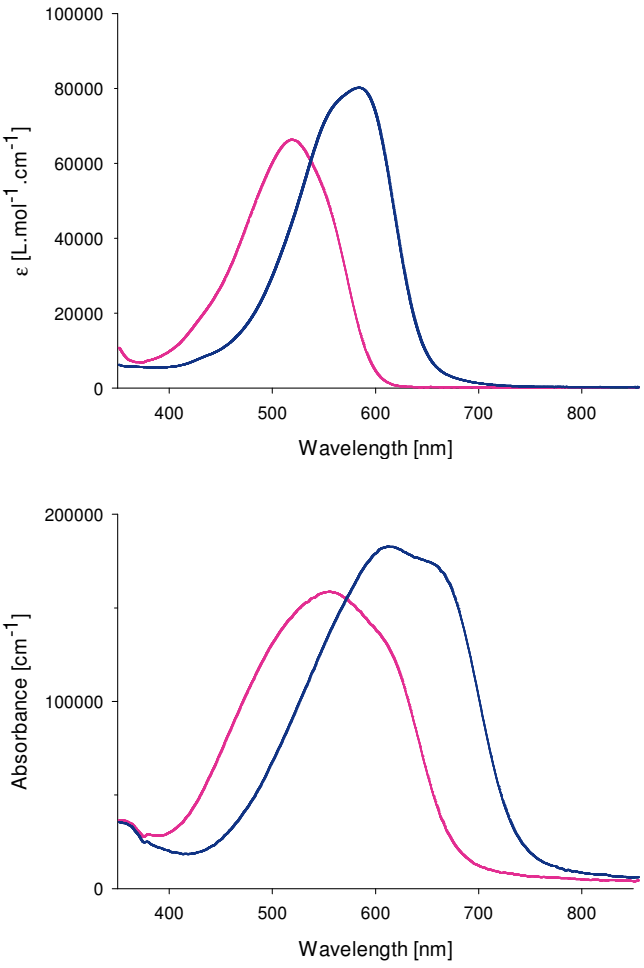

Fig. 5 Absorption spectra of compound **1** (blue line) and **2** (pink line) in CH_2Cl_2 solution (top) and as films of 15 nm thickness evaporated on glass (bottom).

Cyclic voltammetry was performed in CH_2Cl_2 in the presence of Bu_4NPF_6 as supporting electrolyte. The cyclic voltammogram (CV) of **1** exhibits a first one-electron reversible oxidation wave with an anodic peak potential E_{pa}^1 at 0.64 V *vs* Fc/Fc^+, associated to a stable radical cation, and a second irreversible oxidation wave at E_{pa}^2 at 1.21 V *vs* Fc/Fc^+ (Fig. S11 and S12). An irreversible reduction wave is observed with a cathodic peak potential (E_{pc}^1) at -1.33 V. Comparison of the first standard oxidation potentials of **1** and **2**,[19b] shows that the bridging leads to a significant negative shift from 0.84 V to 0.60 V associated with an increase of the HOMO level, whereas no significant change is observed on the reduction potential.

Theoretical calculations based on density functional methods were performed with the Gaussian 09 program for compounds **1** and **2**.[30] Becke's three-parameter[31] gradient-corrected functional (B3LYP) with the 6-311G(d,p) basis set were used to optimize their geometries and to compute their electronic structures at the observed minima. Except the two ethyl chains perpendicular to the conjugated system, molecule **1** shows a planar structure with the two terminal thiophene rings in an *anti* conformation relatively to the central bridged bithiophene core and the two DCV moieties in *syn* conformation relatively to the sulphur atom of the vicinal thiophene.

Fig. 6 compares the HOMO and LUMO energy levels of **1** and **2**. The HOMO and LUMO of both molecules display typical aromatic and quinoid characters, respectively, with a full delocalization on the whole π-conjugated backbone. The bridging of **1** produces a significant increase of the HOMO level (+0.23 eV) compared to **2**, in full agreement with the CV results. On the other hand, the LUMO level of **1** is increased by 0.06 eV. These combined results lead to a 0.17 eV reduction of HOMO-LUMO gap for the bridged system in agreement with optical data.

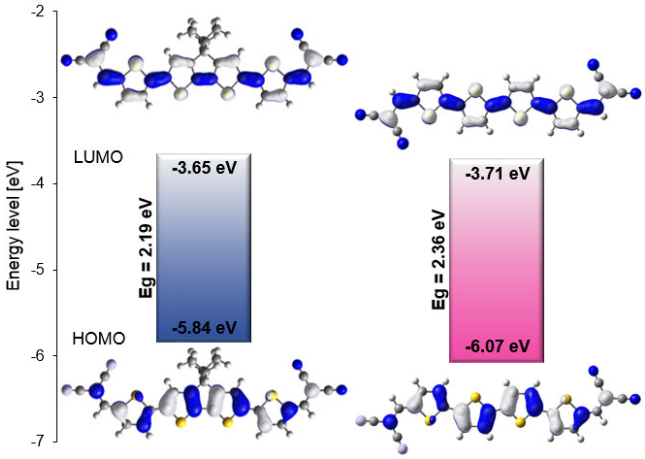

Fig. 6 HOMO and LUMO energy levels and their representations for **1** and **2** after optimization with Gaussian 09 at the B3LYP/6-311G (d,p) level of theory.

The photovoltaic performance of compound **1** as donor material for OPV has been evaluated on simple bi-layer PHJ cells using C_{60} as acceptor material (Fig. 7, top). Cells of 27 mm^2 active area were fabricated by successive thermal evaporations of donor **1**, 20 nm of C_{60} and 150 nm of aluminum on ITO substrates pre-coated with a 40 nm layer of spin-cast PEDOT-PSS (see ESI). Table 1 lists the photovoltaic parameters of the devices under AM 1.5 simulated solar illumination.

Table 1. Photovoltaic parameters of bi-layers donor/C_{60} under AM 1.5 simulated solar illumination with an average power intensity of *ca*. 80 mW cm^{-2}.[a,b]

Entry	Donor	*d* (nm)	V_{oc} (V)	J_{sc} (mA/cm^2)	*FF*	*PCE* (%)
1	**1**	10	0.85 (0.83)	4.00 (3.75)	0.44 (0.43)	**1.89** (1.66)
2	**1**	15	0.97 (0.94)	5.07 (4.88)	0.45 (0.41)	**2.82** (2.34)
3	**1**	20	0.95 (0.94)	4.19 (3.55)	0.39 (0.36)	**1.92** (1.50)
4	**2**	15	0.88 (0.86)	1.74 (1.50)	0.25 (0.24)	**0.51** (0.41)

[a] General structure of the bi-layer solar cells ITO/PEDOT:PSS (40 nm)/Donor/C_{60} (20 nm)/Al (150 nm). [b] Data in brackets are the average values measured on 18, 37, 25 and 22 cells respectively for entries 1, 2, 3 and 4; data in bold are the best of each series (see also ESI).

Comparison of the data of entries 1-3 shows that the maximum values of the short-circuit current density (J_{sc}) and *PCE* values are obtained with a donor layer of 15 nm thickness (*d*). This value could represent the best trade-off between the absorbance of the donor layer, exciton diffusion and charge collection.[32] With this thickness, the best cell gives a J_{sc} of 5.07 mA cm^{-2} and a *PCE* of 2.82% (Fig. 7, middle). Under identical conditions, compound **2** gives a J_{sc} of 1.74 mA cm^{-2} and a *PCE* of 0.51%. The difference in J_{sc} between compounds **1** and **2** can be related to the better absorption properties of **1** which is also observed on the external quantum efficiency (*EQE*) spectra (Fig. 7, bottom). The very low fill-factor (*FF*) recorded for **2** could be related to both hindered charge transport within the active layer and limited charge-transfer at the donor/electrode interface maybe due to a larger extraction barrier related to the deeper HOMO level of **2**.[33]

It is worth noting that in the best conditions, the bridged compound **1** leads to higher values of the open-circuit voltage (V_{oc}) and *FF* than compound **2**. Based on the higher HOMO level of the bridged donor, a decrease of V_{oc} could have been expected.[34] In fact, such concomitant increase of V_{oc} and *FF* caused by the covalent bridging of the donor has already been observed and attributed to changes in the interfacial dipoles at the donor/electrode interface and/or at the donor/acceptor interface,[24c] further work is needed to clarify this question.

Fig. 7 (bottom) shows the *EQE* action spectrum of the best bi-layer PHJ devices based on **1** and **2** under monochromatic irradiation. The spectrum of **2** shows small peaks around 360 nm associated with the contribution of C_{60} followed by a broad band extending from 450-700 nm with a maximum of *ca* 8.0% corresponding to the absorption of the donor. As expected, the spectrum of the cell based on the bridged compound **1** shows a strong enhancement of the photoresponse with a first maximum of 35% at ~ 360 nm due to C_{60} and a second maximum of 38% at ~ 660 nm. On the other hand, a large extension of photo-response

toward longer wavelengths up to 750 nm is observed, in agreement with the reduced band gap of the bridged donor.

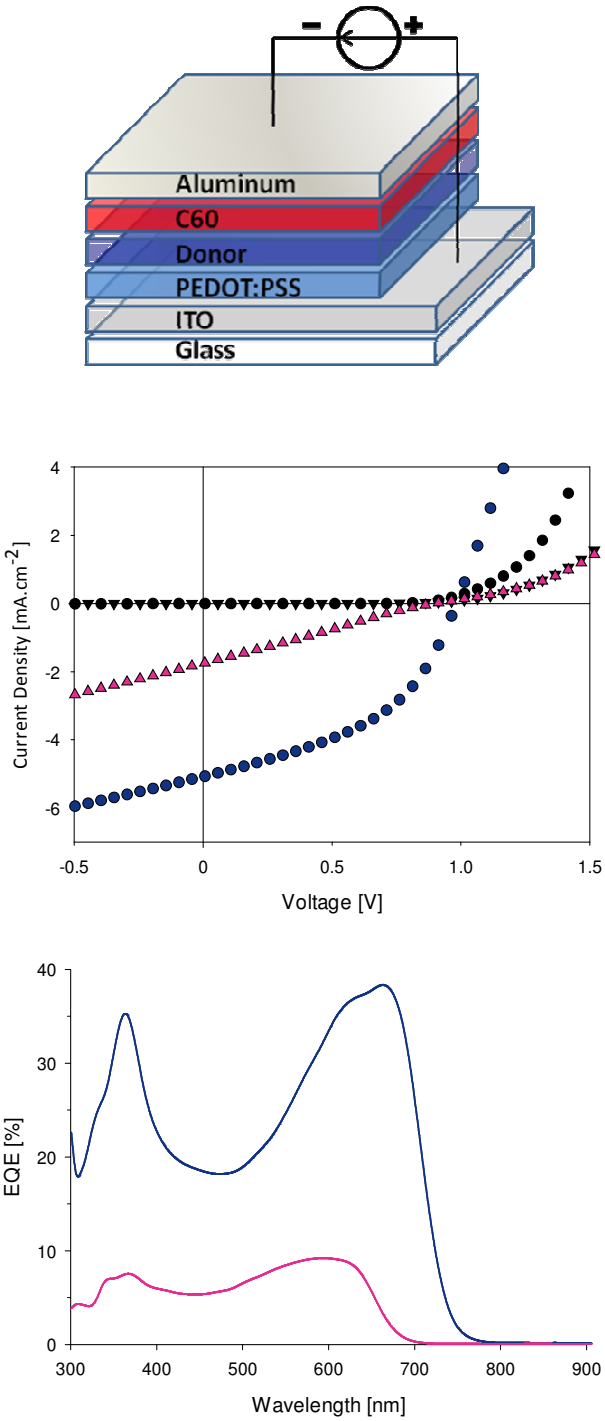

Fig. 7 Top: architecture of bi-layer PHJ solar cells. Middle: current density *vs* voltage curves of bi-layer PHJ cells ITO/PEDOT-PSS/**1** (circles) or **2** (triangles) (15 nm)/C_{60} (20 nm)/Al (150 nm) in the dark (in black) and under AM 1.5 simulated solar light (80 mW cm^{-2}) (in colour). Bottom: external quantum efficiency of the best bi-layer PHJ cells under monochromatic irradiation. Blue line: **1**, pink line: **2**.

The hole mobility (μ_h) of donor **1** has been estimated on hole only devices using the space-charge-limited conduction (SCLC) method (see ESI). The obtained value $\mu_h = 3.4 \times 10^{-5}$ cm^2 V^{-1}s^{-1} is comparable to the values found on many small molecular donors.[1g] In the same conditions as for **1**, the determination of the hole mobility of reference compound **2** leads to a value of 2×10^{-6} cm^2 V^{-1}s^{-1}. The improved electronic charge transport properties of titled compound **1** can contribute to its better OPV performance. On the other hand, these results show also that, while increasing the solubility of compound **1**, the introduction of ethyl substituents does not prevent efficient charge transport in agreement with X-ray data displaying strong intermolecular π-interactions in the solid state.

In previous work on the open-chain donor **2**, a *PCE* of 1.20 % with a J_{sc} of 2.90 mA cm^{-2} was reported for an inverted cell of composition: ITO/C_{60} (15 nm)/**2** (6 nm), 9,9-bis[4-(*N*,*N*-bis-biphenyl-4-ylamino)phenyl]-9H-fluorene (BPAPF) (5 nm)/BPAPF p-doped with NDP9 (a proprietary dopant) (50 nm)/NDP9 (1 nm)/Au (50 nm).[19b] More recently the same group reported a cell of similar architecture with a 6 mm^2 area in which the planar heterojunction was replaced by a thicker layer of co-evaporated donor **2** and C_{60} (20 nm). This multi-layer cell delivered a J_{sc} of 6.49 mA cm^{-2} with a *PCE* of 3.00 %.[35] Comparison of these results with those of Table 1 shows that the introduction of buffer layers of optimized thickness and doping together with the fabrication of a BHJ cell structure can greatly improve the PV performance of devices based on donor **2**.

In order to further investigate the potential of donor **1**, various experiments aiming at optimizing the device have been performed. Attempts to apply thermal treatment to the bi-layer cells remained unsuccessful and only led to a degradation of the performance. More advanced BHJ cells have been prepared by co-evaporating **1** and C_{60} with a spatial gradient of concentration and by inserting a hole extraction layer of 4,4'-bis[*N*-(1-naphtyl)-*N*-phenylamino]biphenyl (α-NPB) at the anode and LiF at the cathode, as described in Fig. 8.[22b]

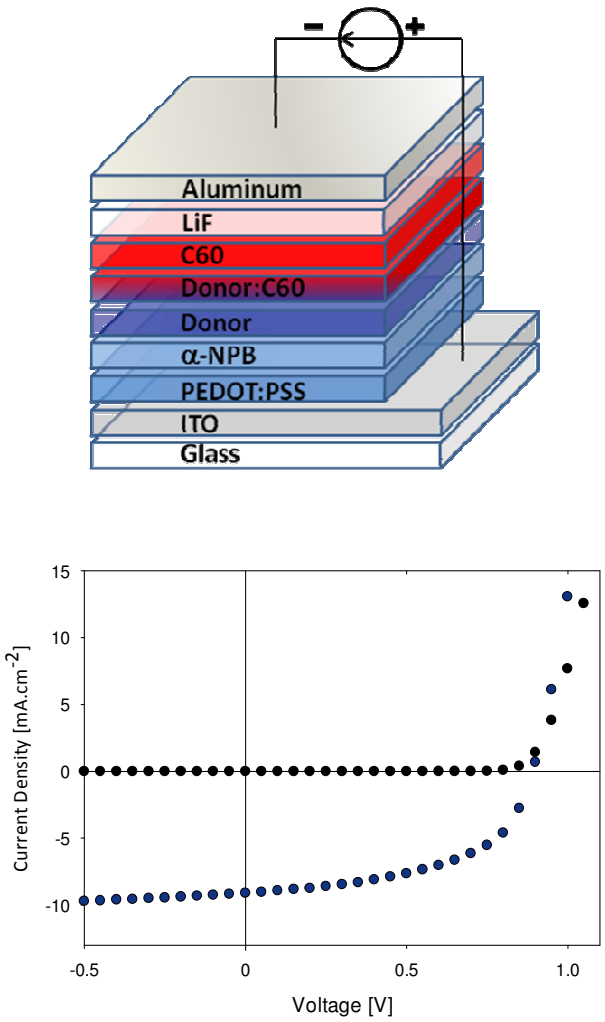

Fig. 8 Top: architecture of a gradiently doped BHJ device: ITO/PEDOT-PSS/α-NPB/**1**/**1**:C_{60} (45 to 70%)/C_{60}/LiF/Al. Bottom: current density *vs* voltage curves in the dark (black circles) and under AM 1.5 simulated solar light (100 mW cm^{-2}) (blue circles).

The cells of 28 mm^2 area have been optimized by: i) varying the thickness of α-NPB, ii) inserting an additional layer of pure **1** before co-evaporation with C_{60} and iii) controlling the gradient of co-evaporation while maintaining a 40:60 ratio of **1** and C_{60}. The best results have been obtained with a device with the following of structure: ITO/PEDOT:PSS (40 nm)/α-NPB (15 nm)/**1** (5 nm)/**1**:C_{60} (45 to 70%) (30 nm)/C_{60} (30 nm)/LiF (1.2 nm)/Al (100 nm). The current density *vs* voltage curves of three cells of this type showed a PCE_{max} of 4.30% (average value of 4.0%) associated with V_{oc}, J_{sc} and *FF* values of 0.89 V, 9.12 mA/cm^2 and 0.53, respectively (Fig. 8). As expected, the corresponding EQE spectrum exhibits an enhanced photocurrent with a plateau of ~52% in the 570-640 nm range (Fig. S15).

Conclusions

A covalently bridged α,ω-bis(dicyanovinyl)quaterthiophene with a central cyclopenta[2,1-*b*:3,4-*b*']dithiophene has been synthesized and purified by standard column chromatography thanks to the improved solubility imparted by ethyl chains introduced on the methylene bridge. Comparison of the electrochemical and optical data to those of an open-chain analogue shows that the bridging of the central 2,2'-bithiophene core produces a significant reduction of the band gap associated with a raising of *ca*. 0.15 eV of the HOMO level. X-Ray diffraction analysis of a single crystal reveals a compact structure in which π-stacked molecules are stabilized by multiple short intermolecular contacts.

The photovoltaic performance of the new donor has been analyzed on basic bi-layer planar hetero-junction cells with C_{60} as acceptor. In these conditions, the results show that the bridged donor leads at the same time to improved current density, voltage and fill factor and thus to conversion efficiency *ca* five times larger than that of the open-chain reference compound. In addition, the value of the hole mobility of the new donor is one order of magnitude higher than that of the open-chain compound. The bridged compound has been used as donor in hybrid hetero-junction cells based on active layers produced by co-evaporation with C_{60} under controlled concentration gradient and involving anode and cathode buffer layers. The *PCE* of 4.30% obtained under simulated solar light provides a further clear confirmation of the interest of covalent rigidification as a powerful synthetic tool for the design of efficient molecular donors with limited structural complexity. Work aiming at the extension of this approach to other classes of molecular donors is now underway in our laboratory and will be reported in future publications.

Experimental

All reagents from commercial sources were used without further purification. Reactions were carried out under nitrogen atmosphere unless otherwise stated. Solvents were dried and purified using standard techniques. Flash chromatography was performed with analytical-grade solvents using Aldrich silica gel (technical grade, pore size 60 Å, 230-400 mesh particle size). Flexible plates ALUGRAM® Xtra SIL G UV_{254} from MACHEREY-NAGEL were used for TLC. Compounds were detected by UV irradiation (Bioblock Scientific) or staining with I_2, unless otherwise stated. NMR spectra were recorded with a Bruker AVANCE III 300 (^{1}H, 300 MHz and ^{13}C, 75 MHz). Chemical shifts are given in ppm relative to TMS and coupling constants *J* in Hz. IR spectra were recorded on a Bruker spectrometer Vertex 70 and UV-Vis spectra with a Perkin Elmer 950 spectrometer. Matrix Assisted Laser Desorption/Ionization was performed on MALDI-TOF MS BIFLEX III Bruker Daltonics spectrometer using dithranol as matrix.

Cyclic voltammetry was performed in 0.10 M Bu_4NPF_6/CH_2Cl_2 (HPLC grade). Solutions were degassed by nitrogen bubbling prior to each experiment. Experiments were carried out in a one-compartment cell equipped with platinum electrodes and a saturated calomel reference electrode (SCE) using a Biologic SP-150 potentiostat with positive feedback compensation. Elemental analyses were performed with a thermo-electron instrument (FLASH 2000, Thermo Scientific). DSC and TGA were performed with TA Instruments Q20 and Q500 respectively.

Synthesis. Compounds **2**,[19b] **3**[28] (see ESI) and **5**[19c] have been synthesized following reported procedures.

(4,4-Diethyl-4H-cyclopenta[1,2-b:5,4-b']dithienyl-2,6-diyl)bis(trimethylstannane) 4. *n*-BuLi (1.6 M in hexanes, 5.73 mL, 9.17 mmol) was added dropwise to **3** (860 mg, 3.67 mmol) in 25 mL of anhydrous THF cooled to -78°C. The mixture was then warmed up to

room temperature and further stirred for 2 h. The reaction mixture was cooled to -78°C and Me_3SnCl (1 M in hexanes, 9.17 mL, 9.17 mmol) was added. The reaction mixture was warmed to room temperature and stirred for 14h. Water and CH_2Cl_2 were added. The organic phase was separated and washed with a saturated $NaHCO_3$ solution and brine, dried with $MgSO_4$ and concentrated under reduced pressure yielding **4** (1.98 g, 3.54 mmol, 96%) as a slightly brown solid. ^{1}H NMR (300 MHz, $CDCl_3$, δ): 6.94 (s, 2H), 1.87 (q, *J*=7.4, 4H), 0.64 (t, *J*=7.4, 6H), 0.37 (s, 18H).

5,5'-(4,4-Diethyl-4H-cyclopenta[1,2-b:5,4-b']dithienyl-2,6-diyl)dithiophene-2-carbaldehyde 7. A mixture of **4** (1.00 g, 1.79 mmol), 5-bromothiophene-2-carbaldehyde **6** (751 mg, 439 mL, 3.93 mmol) and tetrakis(triphenylphosphine)palladium(0) (103 mg, 0.09 mmol) in 40 mL of degassed DMF was stirred at 80°C for 14 h. After cooling, water and CH_2Cl_2 was added. The organic phase was separated and washed with brine, dried with $MgSO_4$ and concentrated under reduced pressure. The crude oil was purified by column chromatography on silica gel (eluent: CH_2Cl_2/petroleum ether 1:1 to CH_2Cl_2) yielding **7** (710 mg, 1.56 mmol, 87%) as a red powder. mp 214°C (onset DSC). ^{1}H NMR (300 MHz, $CDCl_3$, δ): 9.85 (s, 2H), 7.66 (d, *J*=4.0, 2H), 7.24 (d, *J*=4.0, 2H), 7.21 (s, 2H), 1.96 (q, *J*=7.4, 4H), 0.65 (t, *J*=7.4, 6H). ^{13}C NMR (75 MHz, $CDCl_3$, δ): 182.37 (s), 159.39 (s), 147.94 (s), 141.19 (s), 138.45 (s), 137.65 (s), 137.48 (s), 123.48 (s), 120.56 (s), 55.67 (s), 30.30 (s), 9.27 (s). IR (neat): ν = 1645 cm^{-1} (C=O). HRMS (MALDI-TOF): *m/z* calcd. for $C_{23}H_{18}O_2S_4$: 454.0190, found: 454.0197.

2,2'-[(4,4-Diethyl-4H-cyclopenta[1,2-b:5,4-b']dithienyl-2,6-diyl)bis(thiene-5,2-diylmethylylidene)]dipropanedinitrile 1. A solution of **7** (400 mg, 0.88 mmol), malononitrile (175 mg, 2.64 mmol) and triethylamine (9 mg, 12 µL, 0.09 mmol) in 100 mL of

$CHCl_3$ was stirred under reflux for 14 h. The reaction mixture was allowed to cool to room temperature and the solvent was rotary evaporated. The residual powder was purified by column chromatography on silica gel (eluent: CH_2Cl_2/petroleum ether 3:1 to CH_2Cl_2) yielding **1** (456 mg, 823 mmol, 94%) as a dark blue-green powder. mp 303°C (onset DSC). ^{1}H NMR (300 MHz, CD_2Cl_2, δ): 7.80 (s, *J*=0.6, 2H), 7.64 (d, *J*=4.8, 2H), 7.37 (s, 2H), 7.31 (d, *J*=4.2, 2H), 2.00 (d, *J*=7.1, 4H), 0.63 (t, *J*=7.3, 6H). ^{13}C NMR (75 MHz, CD_2Cl_2, δ): 160.93 (s), 150.56 (s), 150.30 (s), 141.31 (s), 140.31 (s), 137.86 (s), 133.79 (s), 124.44 (s), 122.26 (s), 115.08 (s), 114.38 (s), 75.88 (s), 56.39 (s), 30.84 (s), 9.38 (s). IR (neat): ν = 2216 cm^{-1} (C≡N). UV-Vis (CH_2Cl_2): λ_{max} (ε) = 581 nm (80300 L.mol^{-1}.cm^{-1}). HRMS (EI): *m/z* calcd. for $C_{29}H_{18}N_4S_4$: 550.0414, found: 550.0438. Anal. Calc. for $C_{29}H_{18}N_4S_4$: C, 63.25; H, 3.29; N, 10.17; S, 23.29%; found: C, 62.99; H, 3.18; N, 10.05; S, 23.21%.

CCDC 1007813 contains the supplementary crystallographic data for this paper. These data can be obtained free of charge from The Cambridge Crystallographic Data Centre via www.ccdc.cam.ac.uk/data_request/cif.

Acknowledgements

The Ministère de la Recherche is acknowledged for the Ph-D grant to F. Baert. We thank the PIAM of the University of Angers for characterization of organic compounds. Jonhson Mattey is acknowledged for the gift of $PdCl_2$ used for the preparation of $Pd(PPh_3)_4$ catalyst.

References

1 For reviews on molecular OSCs see: (a) M. T. Lloyd, J. M. Anthony and G. C. Malliaras, *Materials Today*, 2007, **10**, 34; (b) J. Roncali, *Acc. Chem. Res*., 2009, 42, 1719; (c) F. Würthner and K. Meerholz, *Chem. Eur. J*., 2010, **16**, 9366; (d) B. Walker, C. Kim and T.-Q. Nguyen, *Chem. Mater*., 2011, **23**, 470; (e) Y. Li, Q. Guo, Z. Li, J. Pei and W. Tian, *Energy Environ. Sci*., 2010, **3**, 1427; (f) A. Mishra and P. Bäuerle, *Angew. Chem. Int. Ed*., 2012, **51**, 2020; (g) Y. Lin, Y. Li and X. Zhan, *Chem. Soc. Rev*., 2012, **41**, 4245; (h) J. Roncali, P. Leriche and P. Blanchard, *Adv. Mater*., 2014, **26**, 3821.

2 (a) Z. He, C. Zhong, X. Huang, W.-Y. Wong, H. Wu, L. Chen, S. Su and Y. Cao, *Adv. Mater.*, 2011, **23**, 4636; (b) L. Dou, J. You, J. Yang, C.-C. Chen, Y. He, S. Murase, T. Moriarty, K. Emery, G. Li and Y. Yang, *Nat. Photon*., 2012, **6**, 180; (c) Z. He, C. Zhong, S. Su, M. Xu, H. Wu and Y. Cao, *Nat. Photon*., 2012, **6**, 591; (d) J. You, L. Dou, K. Yoshimura, T. Kato, K. Ohya, T. Moriarty, K. Emery, C.-C. Chen, J. Gao, G. Li and Y. Yang, *Nat. Commun*., 2013, **4**, 1446; (e) C. Cabanetos, A. El Labban, J. A. Barteld, J. D. Douglas, W. M. Mateker, J. M. J. Fréchet, M. D. McGehee and P. M. Beaujuge, *J. Am. Chem. Soc*., 2013, **135**, 4656.

3 H. K. H. Lee, Z. Li, I. Constantinou, F. So, S. W. Tsang and S. K. So, *Adv. Energy Mater*., 2014, DOI: 10.1002/aenm.201400768.

4 J. Roncali, P. Frère, P. Blanchard, R. de Bettignies, M. Turbiez, S. Roquet, P. Leriche and Y. Nicolas, *Thin Solid Films,* 2006, **511**, 567.

5 (a) Y. Sun, G. C. Welch, W. L. Leong, C. J. Takacs, G. C. Bazan and A. J. Heeger, *Nat. Mater.*, 2011, **11**, 44; (b) A. K. K. Kyaw, D. H. Wang, V. Gupta, J. Zhang, S. Chand, G. C. Bazan and A. J. Heeger, *Adv. Mater.*, 2013, **25**, 2397; (c) V. Gupta, A. K. K. Kyaw, D. H. Wang, S. Chand, G. C. Bazan and A. J. Heeger, *Sci. Rep*., 2013, **3**, 1965; (d) J.E. Coughlin, Z.B. Henson, G.C. Welch and G. Bazan, *Acc. Chem. Res*., 2014, **47**, 257.

6 (a) J. Zhou, X. Wan, Y. Liu, Y. Zuo, Z. Li, G. He, G. Long, W. Ni, C. Li, X. Su and Y. Chen, *J. Am. Chem. Soc*., 2012, **134**, 16345; (b) J. Zhou, Y. Zuo, X. Wan, G. Long, Q. Zhang, W. Ni, Y. Liu, Z. Li, G. He, C. Li, B. Kan, M. Li and Y. Chen, *J. Am. Chem. Soc.*, 2013, **135**, 8484; (c) Y. Chen, X. Wan and G. Long, *Acc. Chem. Res*., 2013, **46**, 2645.

7 Y. Liu, C.-C. Chen, Z. Hong, J. Gao, Y. Yang, H. Zhou, L. Dou, G. Li and Y. Yang, *Sci. Rep*., 2013, **3**, 3356.

8 V. Steinmann, N. M. Kronenberg, M. R. Lenze, S. M. Graf, D. Hertel, K. Meerholz, H. Bürckstümmer, E. V. Tulyakova and F. Würthner, *Adv. Energy Mater*., 2011, **1**, 888.

9 R. Fitzner, E. Mena-Osteritz, A. Mishra, G. Schulz, E. Reinold, M. Weil, C. Körner, H. Ziehlke, C. Elschner, K. Leo, M. Riede, M. Pfeiffer, C. Ulrich and P. Bäuerle, *J. Am. Chem. Soc.*, 2012, **134**, 11064.

10 (a) L.-Y. Lin, Y.-H. Chen, Z.-Y. Huang, H.-W. Lin, S.-H. Chou, F. Lin, C.-W. Chen, Y.-H. Liu and K.-T. Wong, *J. Am. Chem. Soc.*, 2011, **133**, 15822; (b) Y.-H. Chen, L.-Y. Lin, C.-W. Lu, F. Lin, Z.-Y. Huang, H.-W. Lin, P.-H. Wang, Y.-H. Liu, K.-T. Wong, J. Wen, D. J. Miller and S. B. Darling, *J. Am. Chem. Soc*., 2012, **134**, 13616.

11 F. Garnier, *Acc. Chem. Res*., 1999, **32**, 209.

12 G. Barbarella, M. Melucci and G. Sotgiu, *Adv. Mater*., 2005, **17**, 1581.

13 A. Mishra, C.-Q. Ma and P. Bäuerle, *Chem. Rev*., 2009, **109**, 1141.

14 F. Zhang, D. Wu, Y. Xua and X. Feng, *J. Mater. Chem*., 2011, **21**, 17590.

15 N. Noma, T. Tsuzuki and Y. Shirota, *Adv. Mater.*, 1995, **7**, 647.

16 C. Videlot, A. El Kassmi and D. Fichou, *Sol. Energy Mater. Sol. Cell*s, 2000, **63**, 69.

17 R. de Bettignies, Y. Nicolas, P. Blanchard, E. Levillain, J.-M. Nunzi and J. Roncali, *Adv. Mater.*, 2003, **15**, 1939.

18 J. Sakai, T. Taima and K. Saito, *Org. Electron.*, 2008, **9**, 582.

19 (a) K. Schulze, C. Uhrich, R. Schüppel, K. Leo, M. Pfeiffer, E. Brier, E. Reinold and P. Bäuerle, *Adv. Mater*., 2006, **18**, 2872; (b) R. Fitzner, E. Reinold, A. Mishra, E. Mena-Osteritz, H. Ziehkle, C. Korner, K. Leo, M. Riede, M. Weil, O. Tsaryova, A. Weiss, C. Ulrich, M. Pfeiffer and P. Bäuerle, *Adv. Funct. Mater.*, 2011, **21**, 897; (c) R. Fitzner, C. Elschner, C. Uhrich, C. Körner, M. Riede, K. Leo, M. Pfeiffer, E. Reinold, E. Mena-Osteritz and P. Bäuerle, *Adv. Mater.*, 2012, **24**, 675.

20 F. Garnier, R. Hajlaoui, A. El Kassmi, G. Horowitz, L. Laigre, W. Porzio, M. Armanini and F. Provasoli, *Chem. Mater*., 1998, **10**, 3334.

21 (a) A. Yassin, T. Rousseau, P. Leriche, A. Cravino and J. Roncali, *Sol. Energy Mater. Sol. Cell*s, 2011, **95**, 462; (b) D. Demeter, T. Rousseau and J. Roncali, *RSC Advances*, 2013, **3**, 704.

22 (a) V. Jeux, D. Demeter, P. Leriche and J. Roncali, *RSC Advances*, 2013, **3**, 5811; (b) J. W Choi C. H. Kim, J. Pison, A. Oyedele, H. Derbal-Habak, D. Tondelier, A. Leliège, E. Kirchner, P. Blanchard, J. Roncali and B. Geffroy, *RSC Advances*, 2014, **4**, 5236.

23 (a) H. Brisset, C. Thobie-Gautier, A. Gorgues, M. Jubault and J. Roncali, *J. Chem. Soc. Chem. Commun*., 1994, 1765; (b) J. Roncali and C. Thobie-Gautier, *Adv. Mater*., 1994, **6**, 846; (c) P Blanchard, H. Brisset, A. Riou and J. Roncali, *J. Org. Chem.*, 1997, **62**, 2401; (d) J. M. Raimundo, P. Blanchard, N. Gallego-Planas, N. Mercier, I. Ledoux-Rak, R. Hierle and J.

Roncali, *J. Org. Chem.*, 2002, **67**, 205; (e) P. Blanchard, P. Verlhac, L. Michaux, P. Frère and J. Roncali, *Chem. Eur. J.*, 2006, 12, 1244.

24 (a) A. Leliège, C.-H. Le Régent, M. Allain, P. Blanchard and J. Roncali, *Chem. Commun*., 2012, **48**, 8907; (b) A. Leliège, J. Grolleau, M. Allain, P. Blanchard, D. Demeter, T. Rousseau and J. Roncali, *Chem Eur. J*., 2013, **19**, 9948; (c) D. Demeter, V. Jeux, P. Leriche, P. Blanchard, Y. Olivier, J. Cornil, R. Po and J. Roncali, *Adv. Funct. Mater*., 2013, **23**, 4854.

25 Y. Ie, K. Nishida, M. Karakawa, H. Tada, A. Asano, A. Saeki, S. Seki and Y. Aso, *Chem. Eur. J.*, 2011, **17**, 4750.

26 M. Löbert, A. Mishra, C. Uhrich, M. Pfeiffer and P. Bäuerle, *J. Mater. Chem. C*, 2014, **2**, 4879.

27 A. Ojala, H. Bürckstümmer, J. Hwang, K. Graf, B von Vacano, K. Meerholz, P. Erk and F. Würthner, *J. Mater. Chem.*, 2012, **22**, 4473.

28 S. Van Mierloo, P. J. Adriaensens, W. Maes, L. Lutsen, T. J. Cleij, E. Botek, B. Champagne and D. J. Vanderzande, *J. Org. Chem.*, 2010, **75**, 7202.

29 F. Effenberger, F. Würthner and F. Steybe, *J. Org. Chem*., 1995, **60**, 2082.

30 Gaussian 09, Revision A.02, M. J. Frisch, G. W. Trucks, H. B. Schlegel, G. E. Scuseria, M. A. Robb, J. R. Cheeseman, G. Scalmani, V. Barone, B. Mennucci, G. A. Petersson, H. Nakatsuji, M. Caricato, X. Li, H. P. Hratchian, A. F. Izmaylov, J. Bloino, G. Zheng, J. L. Sonnenberg, M. Hada, M. Ehara, K. Toyota, R. Fukuda, J. Hasegawa, M. Ishida, T. Nakajima, Y. Honda, O. Kitao, H. Nakai, T. Vreven, Jr. J. A. Montgomery, J. E. Peralta, F. Ogliaro, V. Bearpark, J. J. Heyd, E. Brothers, K. N. Kudin, V. N. Staroverov, R. Kobayashi, J. Normand, K. Raghavachari, A. Rendell, J. C. Burant, S. S. Iyengar, J. Tomasi, M. Cossi, N. Rega, J. M. Millam, M. Klene, J. E. Knox, J. B. Cross, V. Bakken, C. Adamo, J. Jaramillo, R. Gomperts, R. E. Stratmann, O. Yazyev, A. J. Austin, R. Cammi, C. Pomelli, J. W. Ochterski, R. L. Martin, K. Morokuma, V. G. Zakrzewski, G. A. Voth, P. Salvador, J. J. Dannenberg, S. Dapprich, A. D. Daniels, O. Farkas, J. B. Foresman, J. V. Ortiz, J. Cioslowski and D. J. Fox, Gaussian, Inc., Wallingford CT, 2009.

31 A. D. Becke, *J. Chem. Phys.*, 1993, **98**, 5648.

32 S. M. Menke and R. J. Holmes, *Energy Environ. Sci*., 2014, **7**, 499.

33 A. Guerrero, S. Loser, G. Garcia-Belmonte, C. J. Bruns, J. Smith, H. Miyauchi, S. I. Stupp, J. Bisquert and T. J. Marks, *Phys. Chem. Chem. Phys*., 2013, **15**, 16456.

34 C. J. Brabec, A. Cravino, D. Meissner, N. S. Sariciftci, T. Fromhertz, M. T. Rispens, L. Sanchess and J. C. Hummelen, *Adv. Funct. Mater.*, 2001, **11**, 374.

35 C. Koerner, C. Elschner, N. C. Miller, R. Fitzner, F. Selzer, E. Reinold, P. Bäuerle, M. F. Toney, M. D. McGehee, K. Leo and M. Riede, *Org. Electron.*, 2012, **13**, 623.

Table of contents

Covalent bridging of the central 2,2'-bithiophene of α,ω-bis(dicyanovinyl)quaterthiophene derivatives leads to a reduced band gap and efficient organic solar cells